www.springer.com/41230
https://doi.org/10.1007/s41230-022-2001-6
Research & Development
Vol. 19 No. 5 September 2022
CHINA FOUNDRY

Effect of V and Sn on microstructure and mechanical properties of gray cast iron

Yi-li Li[1], *Rui-run Chen[1], **Qi Wang[1], Wen-chao Cao[1], Xin-xiu Wang[1], Yuan Xia[2], Guo-ping Zhou[2], Ying-dong Qu[3], and Guang-long Li[3]

1. School of Materials Science and Engineering, Harbin Institute of Technology, Harbin 150001, China

2. Yangzhou Wutingqiao Cylinder Liner Co., Ltd., Yangzhou 225000, Jiangsu, China

3. School of Materials Science and Engineering, Shenyang University of Technology, Shenyang 110870, China

Abstract: The cylinder liner is one of the important parts of a diesel engine. Gray cast iron is the main material for manufacturing cylinder liners due to its good casting performance, convenient processing performance, good wear resistance and low cost. In the present work, the effects of vanadium (V) and tin (Sn) on the microstructure and properties of gray cast iron were studied. Results show that increasing the contents of V and Sn can not only refine the graphite, but also reduce the pearlite lamellar space. The graphite size and lamellar spacing of pearlite are firstly reduced and then increased. Pearlite quantity reaches over 98% after adding V and Sn. Adding V and Sn can promote the precipitation and solid solution strengthening of gray cast iron, so as to improve the mechanical properties. The Brinell hardness reaches the peak of 424 HB at the contents of 0.21wt.% V and 0.06wt.% Sn, and the sample containing 0.11wt.% V and 0.08wt.% Sn shows the highest compressive strength and tensile strength of 1,699 MPa and 515 MPa, respectively. The main strengthening mechanism comes from the solid solution strengthening and fine grain strengthening of V and Sn.

Keywords: V; Sn; gray cast iron; cylinder liner; microstructure; mechanical properties

CLC numbers: TG143.2 **Document code:** A **Article ID:** 1672-6421(2022)05-427-08

1 Introduction

The performance of an engine is significantly impacted by the quality of the cylinder liner, one of its key components. Gray cast iron has low cost (20%–40% cheaper than steel) and many desirable properties such as good castability, machining property, and wear resistance [1-6]. Due to the special graphite morphology, gray cast iron has a perfect combination of good mechanical properties and thermal conductivity, therefore, is widely used in engine cylinder liners [7, 8]. With the rapid development of the industry, cylinder liners are required to work at higher and higher temperature and pressure, which will easily lead to the failure of cylinder liners [9]. Strict service environment puts forward high requirements for cast iron materials, such as high strength and hardness, high thermal fatigue resistance, and so on [10]. Therefore, how to optimize the performance of gray cast iron materials is one of the urgent problems that need to be solved.

It is well known that the microstructure plays a vital role in the mechanical properties of alloys [11, 12], and alloying is an effective method to improve the microstructure [13, 14]. Some carbide forming enhancing elements, such as Ti combined with W or Cr, or W together with C, were used to improve the hardness and tensile strength of gray cast iron [15, 16]. Furthermore, some studies have indicated that combining elements that substantially promote pearlite refinement (V and Mo) with those that promote pearlite formation (Sn, Sb, Cu, and Cr) can result in an obvious increase of strength at a relatively lower overall alloying quantity [17]. As it is well known, V is also a strong carbide-forming element, and adding V into gray cast iron can refine the carbides [18, 19]. In addition, V can combine with C to form vanadium carbide with high hardness, high strength and wear resistance, so as to improve the plasticity and toughness of the alloy [20-23]. As a pearlite promoting element, the addition of 0.1wt.% Sn would produce a completely pearlitic matrix and consequently improve the tensile strength of both gray and nodular irons [24-25]. Even though the addition of V or Sn into

***Rui-run Chen**

Male, born in 1975, Ph. D., Professor, Dean. His research interests mainly focus on the casting process and Nb-Si alloy.

E-mail: ruiruncheh@hit.edu.cn

****Qi Wang**

E-mail: wangqi_hit@hit.edu.cn

Received: 2022-01-11; Accepted: 2022-07-08

gray cast iron has been well investigated, the impact of their co-effect has not been well defined.

The aim of the present study is to investigate the effect of V and Sn addition on the microstructure, hardness and strength of the gray cast irons used in a super large cylinder liner (with a diameter greater than 270 mm). Gray cast irons with different V and Sn additions were designed, with a small amount of phosphorus (P) (less than 0.3wt.%) to improve the wear resistance of castings, and correspondingly, the microstructures and mechanical properties were tested. Based on the experimental results, the optimal chemical composition of gray cast iron with trace V and Sn addition was obtained, and applied to the production of a super large cylinder liner.

2 Experimental procedure

The gray cast irons were prepared in a medium frequency induction furnace (50 kW) with a capacity of 10 kg, and Y-block specimens (Fig. 1) were poured at 1,650–1,750 K in iron molds. The V (0.11wt.%, 0.16wt.%, 0.21wt.%) and Sn (0.04wt.%, 0.06wt.%, 0.08wt.%) were added in the form of FeV50 and refined Sn (99% purity), respectively. The inoculant used in the experiment is the silicon-barium inoculant supported by Yixing Jiahu Furnace Charge Co., Ltd. The chemical compositions of all the specimens are shown in Table 1, and Fe is the balance.

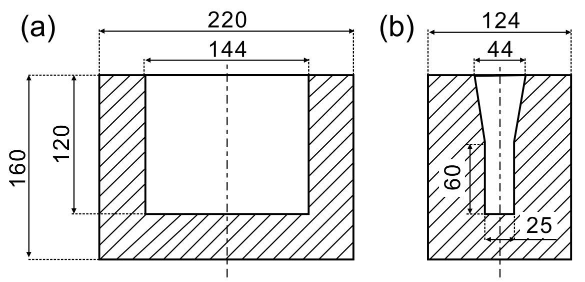

Fig. 1: Schematic of Y-type block (mm): (a) main view; (b) side view

Table 1: Chemical composition of specimens (wt.%)

Sample No.	C	Si	Mn	P	S	V	Sn
1	2.98	1.89	0.68	0.25	0.04	0.01	0
2	2.89	1.93	0.67	0.23	0.05	0.11	0.04
3	2.95	1.95	0.71	0.26	0.04	0.11	0.06
4	3.03	1.91	0.66	0.24	0.06	0.11	0.08
5	2.87	2.03	0.73	0.25	0.04	0.16	0.04
6	3.05	1.97	0.68	0.27	0.05	0.16	0.06
7	2.96	2.04	0.71	0.26	0.05	0.16	0.08
8	2.91	2.01	0.64	0.25	0.06	0.21	0.04
9	3.01	1.98	0.72	0.21	0.04	0.21	0.06
10	2.99	1.94	0.69	0.28	0.04	0.21	0.08

For X-ray diffractometer (XRD) metallographic analysis, the samples of 10 mm×10 mm×10 mm were cut from the lower end of the Y-type blocks, and subsequently polished with various multiples of grit papers. Empyrean XRD was employed to analyze the phase constitutions. The diffractometer was carried out via Cu Kα radiation with the scanning angle from 10° to 90°, and the scanning speed was 8°·min^{-1}. The microstructure observation was carried out by means of optical microscopy (OM) and ZEISS scanning electron microscopy (SEM). The metallographic samples were polished to observe the morphology and content of graphite and pearlite. After being corroded by 4vol.% nitric acid alcohol, scanning electron microscopy was used to observe the lamellar pearlite.

The hardness tests were performed using a 320 HBS-3000 Brinell hardness tester under 750 kg load holding for 30 s, with a 5 mm indenter. Five measurements were made on each sample to obtain the average value. The compressive strength and tensile strength tests were carried out by using Instron 5569 electronic universal testing machine at a strain rate of 1 mm·min^{-1} and 0.5 mm·min^{-1}, respectively. The dimensions for the sample for compressive strength testing is Φ6 mm×9 mm, and the shape for the sample for tensile strength testing is shown in Fig. 2. Three samples were tested under each condition, and the results were obtained by taking the average.

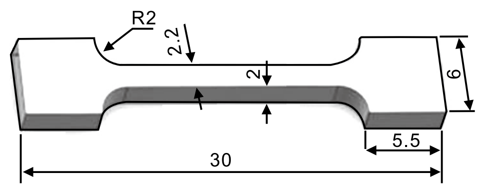

Fig. 2: Tensile test specimen (mm)

3 Results and discussion

3.1 Phase constitution

Samples containing different contents of V and Sn were selected as representatives for XRD analysis, and the test results are shown in Fig. 3.

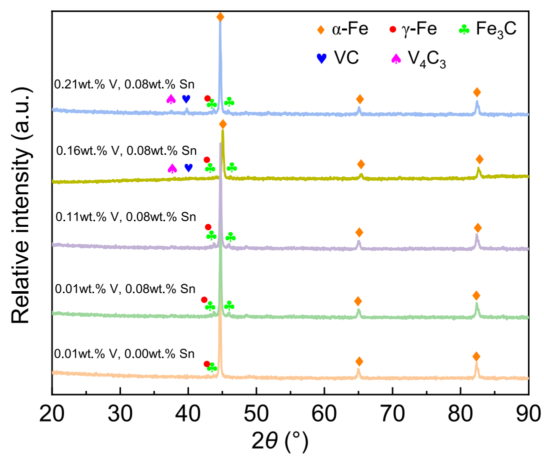

Fig. 3: X-ray diffraction analysis results

After adding a certain amount of V and Sn elements, the structure of the samples is still mainly composed of ferrite and a certain amount of austenite and cementite. When the V content increases to 0.16wt.%, VC and V_4C_3 appear. In addition, no Sn related substances are found, indicating that the addition amount of Sn is too small to be detected.

3.2 Microstructure

Figure 4 reveals the typical morphologies of graphite observed by OM for all the samples containing different contents of V and Sn before corroded. The dark area is flake graphite, and the bright area is the matrix. It can be seen from Fig. 4 that there is not only A-type graphite, but also some D-type and E-type graphites in the structure. The size of graphite was rated according to GB/T 7216-2009 (higher grade means smaller graphite size) and the results are shown in Table 2. It can be found that the addition of alloy elements has a great impact on the graphite size. The graphite is the smallest in the sample with 0.11wt.% V and 0.08wt.% Sn, as shown in Table 2. When 0.11wt.% V is added, in the early stage of solidification, V is firstly combined with carbon in the melt to generate a great number of dispersed and uniformly distributed V carbide particles. These particles act as the second phase particles in the subsequent eutectic reaction, hindering the growth of crystal grains and promoting the uniform distribution of graphite [26]. At the same time, due to its strong positive segregation effect,

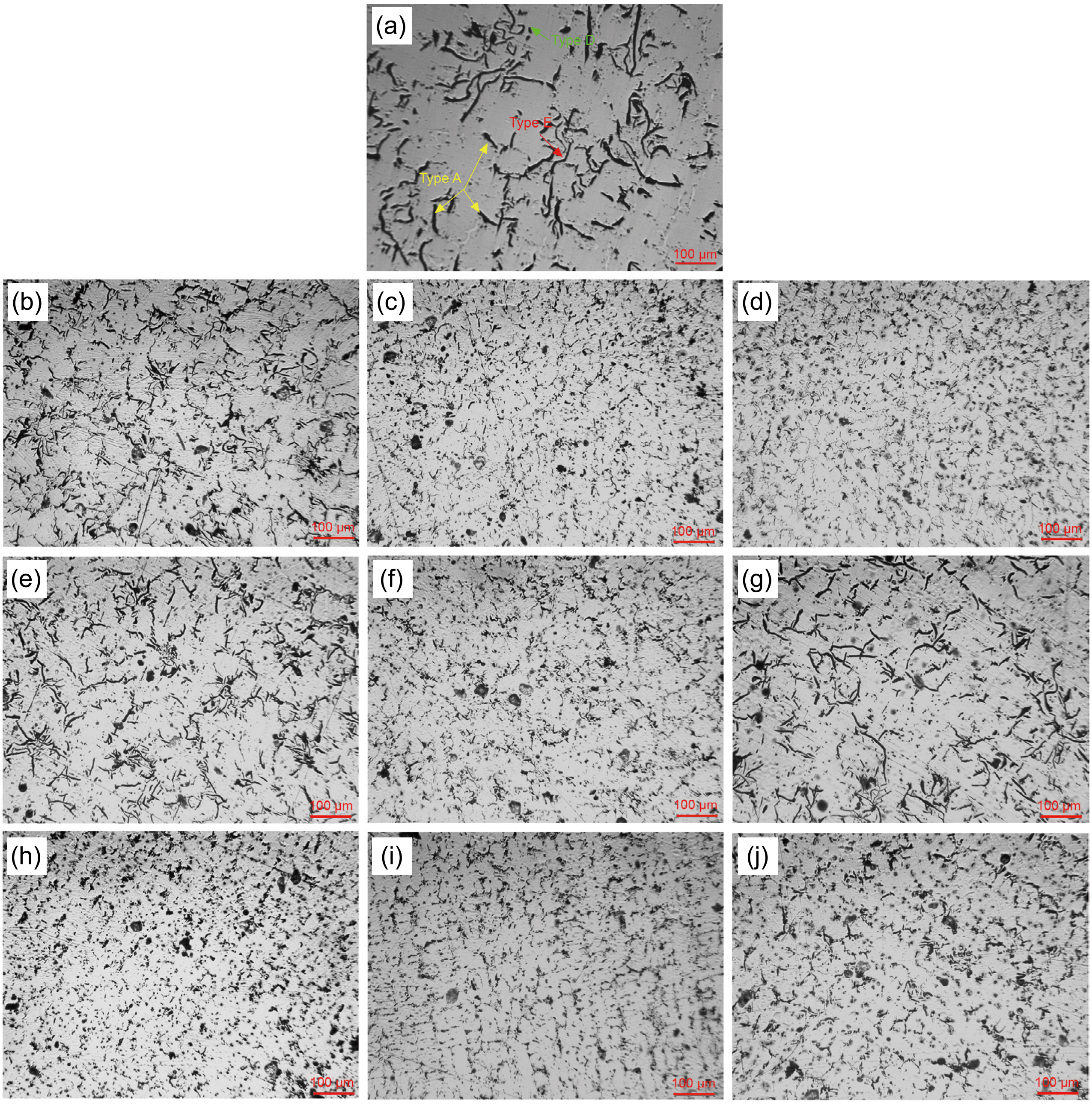

Fig. 4: OM of gray cast iron graphite structure with different contents of V and Sn: (a) 0.01wt.% V, 0.00wt.% Sn; (b) 0.11wt.% V, 0.04wt.% Sn; (c) 0.11wt.% V, 0.06wt.% Sn; (d) 0.11wt.% V, 0.08wt.% Sn; (e) 0.16wt.% V, 0.04wt.% Sn; (f) 0.16wt.% V, 0.06wt.% Sn; (g) 0.16wt.% V, 0.08wt.% Sn; (h) 0.21wt.% V, 0.04wt.% Sn; (i) 0.21wt.% V, 0.06wt.% Sn; (j) 0.21wt.% V, 0.08wt.% Sn

Table 2: Graphite structure rating table

Alloying element (wt.%)	0.01 V, 0.00 Sn	0.11 V, 0.04 Sn	0.11 V, 0.06 Sn	0.11 V, 0.08 Sn	0.16 V, 0.04 Sn	0.16 V, 0.06 Sn	0.16 V, 0.08 Sn	0.21 V, 0.04 Sn	0.21 V, 0.06 Sn	0.21 V, 0.08 Sn
Graphite grade	3	4	5–6	6–7	4	5–6	4	5–6	5–6	4–5

Sn will stably remain at the front of the unsolidified melt and hinder the growth of graphite [27]. When too much V (greater than 0.11wt.%) is added, V atoms prevent the diffusion of C atoms, that is, preventing the precipitation of graphite phase, making the flake graphite coarsen. In addition, V increases the undercooling of molten iron, and also contributes to the formation of coarse graphite.

Figure 5 shows the OM structure of gray cast iron castings containing different contents of V and Sn after corrosion by 4vol.% nitric acid and alcohol. The dark gray phase around the black graphite is ferrite and the light gray phase is pearlite. It can be seen from Fig. 5 that all the samples present a fully pearlitic matrix. When the V content is 0.21wt.%, the ferrite content decreases while the pearlite content increases with the increase

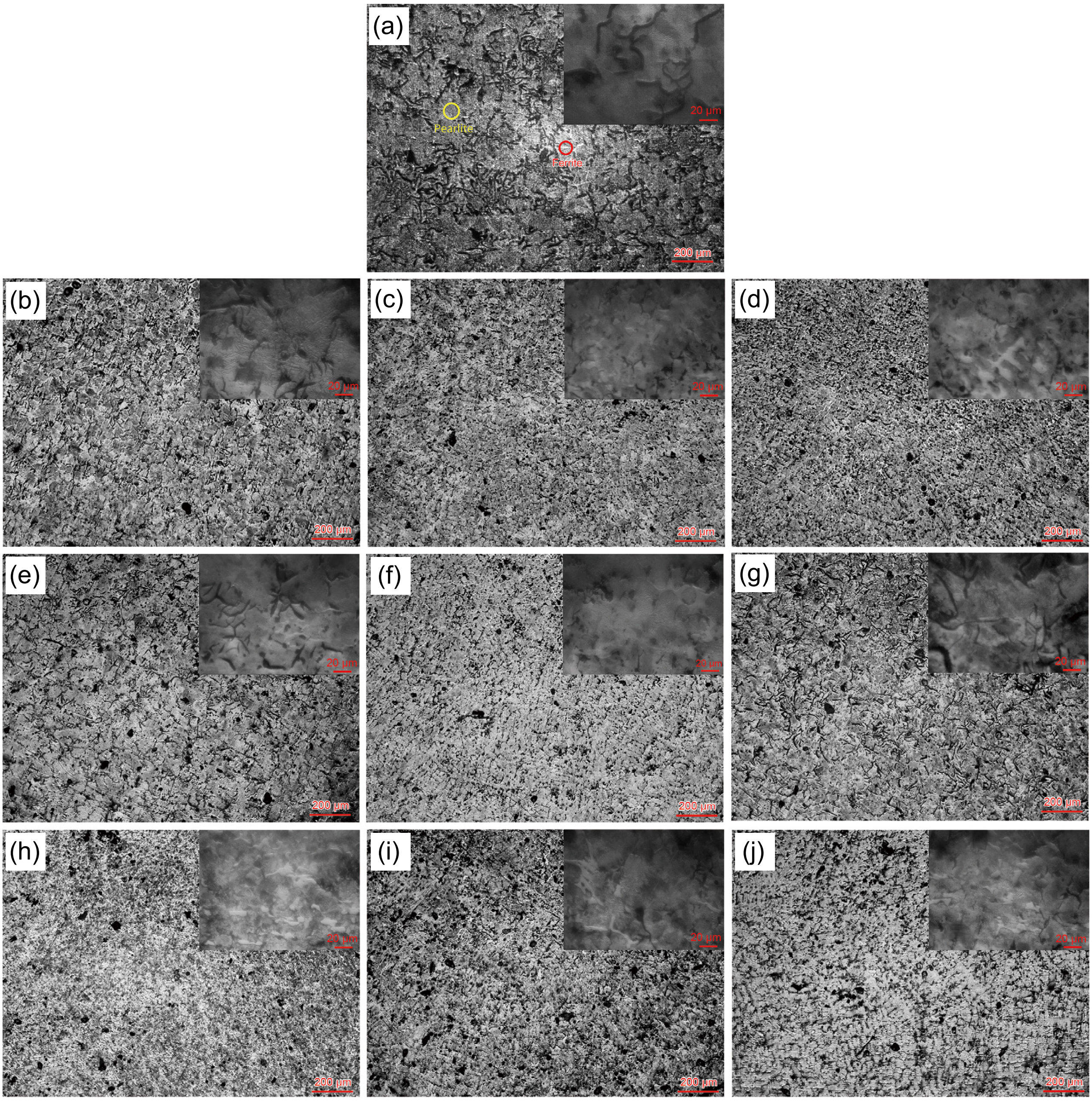

Fig. 5: OM structure of the cast irons with different contents of V and Sn: (a) 0.01wt.% V, 0.00wt.% Sn; (b) 0.11wt.% V, 0.04wt.% Sn; (c) 0.11wt.% V, 0.06wt.% Sn; (d) 0.11wt.% V, 0.08wt.% Sn; (e) 0.16wt.% V, 0.04wt.% Sn; (f) 0.16wt.% V, 0.06wt.% Sn; (g) 0.16wt.% V, 0.08wt.% Sn; (h) 0.21wt.% V, 0.04wt.% Sn; (i) 0.21wt.% V, 0.06wt.% Sn; (j) 0.21wt.% V, 0.08wt.% Sn

Table 3: Statistical results of pearlite content calculated by Image Pro

Alloying element (wt.%)	0.01 V, 0.00 Sn	0.11 V, 0.04 Sn	0.11 V, 0.06 Sn	0.11 V, 0.08 Sn	0.16 V, 0.04 Sn	0.16 V, 0.06 Sn	0.16 V, 0.08 Sn	0.21 V, 0.04 Sn	0.21 V, 0.06 Sn	0.21 V, 0.08 Sn
Pearlite content (%)	90	98	98	98	99	99	98	98	98	99

of Sn. As shown in Table 3, when V content is 0.01wt.% and Sn content is 0wt.%, the content of pearlite is 90%. This content increases to 98%–99%, with the increase of V and Sn. With the increase of V and Sn, carbides appear at the boundary between graphite and austenite, resulting in a strong strengthening effect [25]. As a result, the area around the graphite retains enough C atoms to form pearlite instead of ferrite [25].

The pearlite structures in all the samples are shown in Fig. 6. It is found from the figure that the obtained pearlites are all lamellar pearlites. The pearlite spacing in the sample containing 0.01wt.% V is about 750 nm. With the increase of V from 0.11wt.% to 0.21wt.% and Sn content remaining unchanged, the lamellar spacing decreases firstly and then increases slightly. When the content of V is 0.16wt.% and that of Sn is 0.06wt.%, the lamellar spacing reaches the minimum, about 112 nm. V can form carbides in various temperature ranges, and these carbides serve as the nuclei to promote the precipitation of pro-eutectic austenite, and then refine the pro-eutectic austenite [23]. After the eutectoid reaction, a pearlite matrix with fine grains and lamellar spacing can be obtained, and the pearlite structure is strengthened and refined. In addition, the Sn element enriched around the graphite structure can prevent the carbon in the austenite from

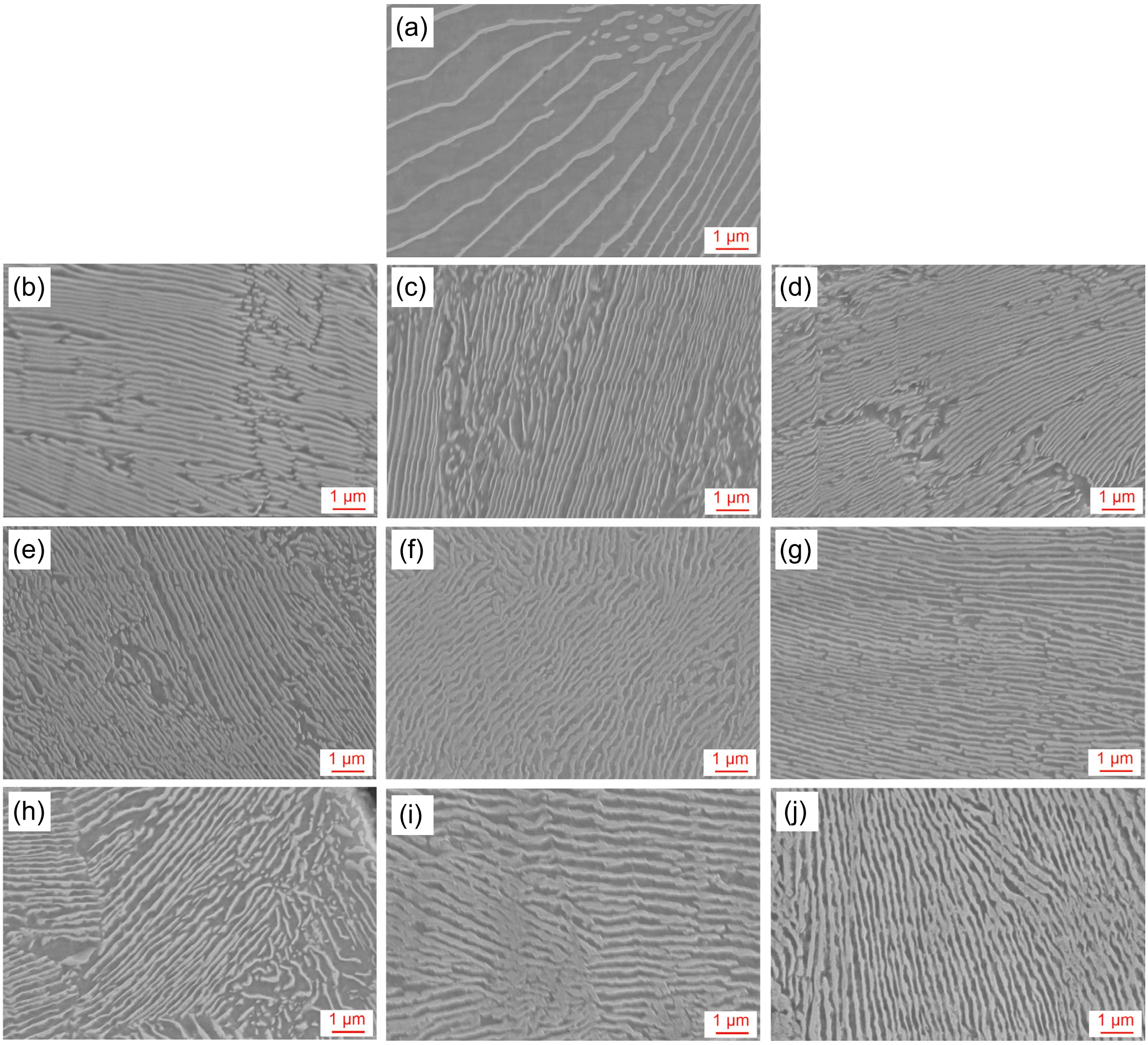

Fig. 6: SEM image of gray cast iron pearlite structure with different contents of V and Sn: (a) 0.01wt.% V, 0.00wt.% Sn; (b) 0.11wt.% V, 0.04wt.% Sn; (c) 0.11wt.% V, 0.06wt.% Sn; (d) 0.11wt.% V, 0.08wt.% Sn; (e) 0.16wt.% V, 0.04wt.% Sn; (f) 0.16wt.% V, 0.06wt.% Sn; (g) 0.16wt.% V, 0.08wt.% Sn; (h) 0.21wt.% V, 0.04wt.% Sn; (i) 0.21wt.% V, 0.06wt.% Sn; (j) 0.21wt.% V, 0.08wt.% Sn

being deposited into the graphite structure during the eutectoid transformation process, thereby promoting the formation of the pearlite. To sum up, the addition of V and Sn shortens the lamellar spacing of pearlite compared to the sample with 0.01wt.% V and 0wt.% Sn, and makes the pearlite more refined.

3.3 Mechanical properties

The mechanical properties of gray cast iron castings with different V and Sn contents were tested, and the test results are shown in Fig. 7.

It can be clearly seen in Fig. 7(a) that when the V content is 0.01wt.% and 0.11wt.%, the hardness of the samples is basically proportional to the Sn content. The minimum Brinell hardness value for the sample containing 0.01wt.% V is 236 HB, and the maximum hardness reaches 424 HB when 0.21wt.% V and 0.06wt.% Sn are added, which increases about 79.66% compared to the sample without Sn and V addition. The increase of the hardness is attributed to the increase of matrix hardness and the precipitation of vanadium carbide [22]. The addition of V and Sn refines the graphite and the pearlite structure. According to the Hall-Petch relationship, the low graphite and the increasing pearlite in the sample are beneficial for the improvement of Brinell hardness [28, 29]. It can be found from the XRD diagram that vanadium carbides appear after adding V, as shown in Fig. 3, which gradually improves the hardness of the matrix. The number of reinforcing particles in the structure is increased, which will make the movement of dislocations difficult, and plays a role of precipitation strengthening to a certain extent [30, 31]. Ahiale et al. [25, 32] studied the effect of V addition on the hardness of the cast iron and also found that the formation of vanadium carbides leads to an increase in hardness.

Figure 7(b) shows the compressive strength of the samples prepared with various alloying elements. When the V content increases from 0.01wt.% to 0.11wt.%, the compressive strength increases with the increase of Sn. The compressive strength of samples after adding V and Sn is significantly higher than that sample only containing 0.01wt.% V. When the V content reaches 0.11wt.% and the Sn content reaches 0.08wt.%, the compressive strength reaches the highest value of 1,699 MPa, which is about 64.79% higher than the raw material. According to Tables 2 and 3, it can be found that the microstructural features play a crucial role in increasing the compressive strength. First of all, the finer the graphite, the lesser its splitting effect on the matrix. Adding V and Sn can refine the matrix structure, so the compressive strength can be improved. Moreover, the solid solution of V also can strengthen the pearlite matrix and prevent the cracks from propagating along the matrix, thereby increasing the compressive strength.

The relationship between alloying elements and the tensile strength of all the samples are shown in Fig. 7(c). Similar to the compressive strength, the tensile strength of samples also basically increases with the increase of V. The maximal tensile strength appears when V content is 0.11wt.% and Sn content is 0.08wt.%, which is 69.41% higher than that without V and Sn. As can be seen from Fig. 7, the properties of the sample with 0.16wt.% V and 0.08wt.% Sn decrease obviously, due to its graphite being relatively coarser and longer, as shown in Fig. 4. As it is well known, the properties of gray cast iron depend on the morphology of matrix and graphite, especially graphite. The thicker and larger the graphite in size, the worse the performance of the cast iron. The pearlite lamellar spacing is the key factor affecting the tensile strength. The shorter the inter-lamellar spacing in pearlite colonies, the higher the strength [33]. It can be seen from Fig. 6 that the addition of V and Sn obviously refines the pearlite, which contributes to the increase of mechanical properties. The finer the graphite, the greater the tensile strength of the sample [33]. Besides, with the increase of the alloying element content, the number of pearlite also increases, and the soft ferrite structure almost disappears, resulting in the increase of strength. When it reaches a certain degree, the strength will not further increase or even decrease [34, 35]. In addition, in the slow stretching process, when the free cementite reaches its sliding limit, it will begin to hinder the dislocation, thereby improving the tensile strength.

Figure 8 shows the SEM images of the tensile fracture of gray cast iron with different contents of V and Sn. It can be seen that the fracture mode of the casting is brittle fracture, the morphology has the characteristics of obvious cleavage fracture, and there are a great number of tear edges in the fracture structure, as indicated by the red arrows in the figure. After the addition of V and Sn, the river pattern increases at the tensile fracture surface of the samples and a few dimples appear as shown by the yellow arrows in the figure, but it is

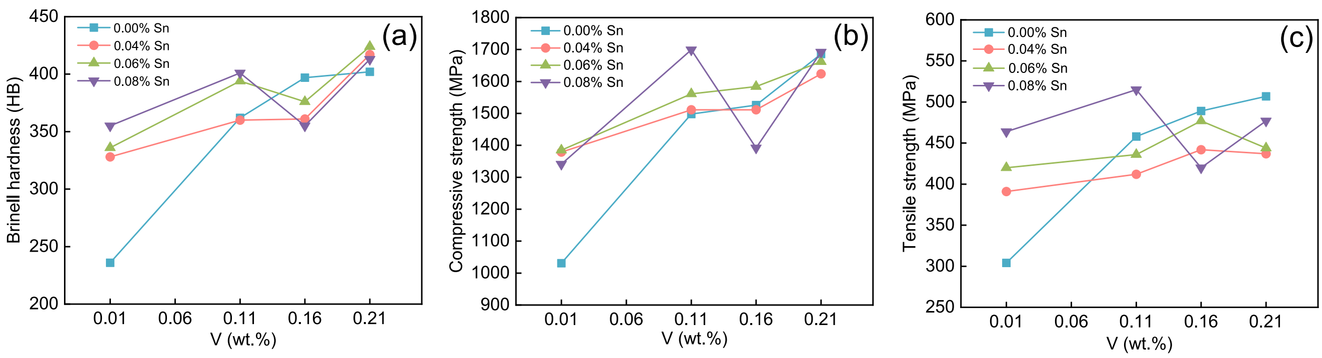

Fig. 7: Effect of V and Sn content on mechanical properties: (a) Brinell hardness; (b) compressive strength; (c) tensile strength

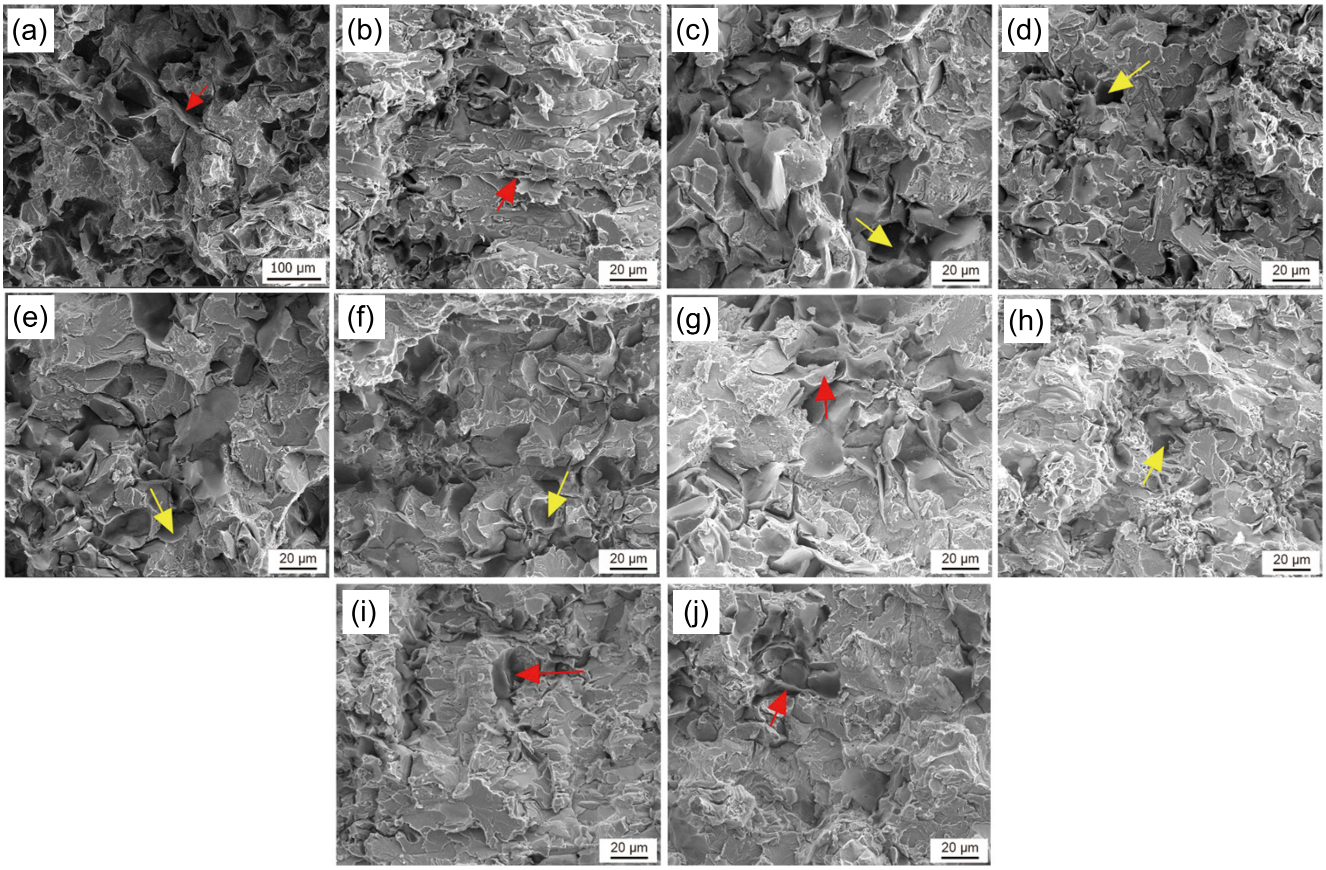

Fig. 8: Fracture of gray cast iron with different contents of V and Sn: (a) 0.01wt.% V, 0.00wt.% Sn; (b) 0.11wt.% V, 0.04wt.% Sn; (c) 0.11wt.% V, 0.06wt.% Sn; (d) 0.11wt.% V, 0.08wt.% Sn; (e) 0.16wt.% V, 0.04wt.% Sn; (f) 0.16wt.% V, 0.06wt.% Sn; (g) 0.16wt.% V, 0.08wt.% Sn; (h) 0.21wt.% V, 0.04wt.% Sn; (i) 0.21wt.% V, 0.06wt.% Sn; (j) 0.21wt.% V, 0.08wt.% Sn

still cleavage fracture. In addition, there are some curved tear edges in some areas, indicating the plasticity of the obtained gray cast irons is slightly improved.

4 Conclusions

Gray cast irons with different contents of V and Sn were prepared, and the microstructure and mechanical properties of the cast irons were investigated. The following conclusions can be drawn:

(1) The addition of V and Sn promotes graphitization, which can not only refine the graphite, but also reduce the pearlite lamellar spacing. The graphite in all the samples is flake graphite.

(2) The V and Sn elements have a positive effect on the Brinell hardness of gray cast irons. When the V content is constant, the hardness basically increases with the increase of Sn. The hardness reaches the peak of 424 HB at 0.21wt.% V and 0.06wt.% Sn.

(3) When the V content is 0.11wt.% and the Sn content is 0.08wt.%, the compressive strength and tensile strength of the gray cast iron reach the maximums of 1,699 MPa and 515 MPa, respectively. The sample with 0.11wt.% V and 0.08wt.% Sn has the best overall performance: its Brinell hardness, compressive strength and tensile strength are 403 HB, 1,699 MPa and 515 MPa, respectively.

(4) The addition of V and Sn can refine graphite, stabilize the pearlite, reduce pearlite lamellar spacing, and strengthen the matrix. The main strengthening mechanism comes from the solid solution strengthening and fine grain strengthening of V and Sn.

Acknowledgements

The authors gratefully acknowledge the financial support from the Jiangsu Innovation and Entrepreneurship Team Foundation, the National Natural Science Foundation of China (No. 51825401), and the Natural Science Foundation of Heilongjiang Province of China (No. LH2020E032).

References

[1] Collini L, Nicoletto G, Ná R K. Microstructure and mechanical properties of pearlitic gray cast iron. Materials Science & Engineering A, 2008, 488(1–2): 529–539.

[2] Stefanescu D M, Suarez R, and Kim S B. 90 years of thermal analysis as a control tool in the melting of cast iron. China Foundry, 2020, 17(2): 69–84.

[3] Wang W, Jing T, Gao Y. Properties of a gray cast iron with oriented graphite flake. Journal of Materials Processing Technology, 2007, 182(26): 593–597.

[4] Zhang M X, Pang J C, Qiu Y, et al. Thermo-mechanical fatigue property and life prediction of vermicular graphite iron. Materials Science & Engineering, A, 2017, 698: 63–72.

[5] Schoenborn S, Kaufmann H, Sonsino C M, et al. Cumulative damage of high-strength cast iron alloys for automotive applications. Procedia Engineering, 2015, 101: 440–449.

[6] Riposan I, Stan S, Chisamera M, et al. Simultaneous thermal and contraction/expansion curves analysis for solidification control of cast irons. China Foundry, 2020, 17(2): 96–110.

[7] Górny M, Kawalec M. Effects of titanium addition on microstructure and mechanical properties of thin-walled compacted graphite iron castings. Journal of Materials Engineering & Performance, 2013, 1519–1524.

[8] Bazdar M, Abbasi H R, Yaghtin A H, et al. Effect of sulfur on graphite aspect ratio and tensile properties in compacted graphite irons. Journal of Materials Processing Technology, 2009, 209(4): 1701–1705.

[9] Liu Y Z, Li Y F, Xing J D, et al. Effect of graphite morphology on the tensile strength and thermal conductivity of cast iron. Materials Characterization, 2018, 144: 155–165.

[10] Pan S N, Zeng F Z, Su N G, et al. The effect of niobium addition on the microstructure and properties of cast iron used in cylinder head. Journal of Materials Research and Technology, 2020, 9(2): 1509–1518.

[11] Saxena K K, Suresh K S, Kulkarni R V, et al. Hot deformation behavior of Zr-1Nb alloy in two-phase region – Microstructure and mechanical properties. Journal of Alloys and Compounds, 2018: 281–292.

[12] Liu Q Y, Zhang X F, Sun Y C, et al. Quantitative models for microstructure and thermal conductivity of vermicular graphite cast iron cylinder block based on cooling rate. China Foundry, 2021, 18(1): 52–59.

[13] Saxena K K, Pancholi V, Chaudhari G P, et al. Hot deformation behaviour and microstructural evaluation of Zr-1Nb alloy. Materials Science Forum, 2016, 890: 319–322.

[14] Kumar B K, Saxena K K, Dey S R, et al. Peak stress studies of hot compressed TiHy 600 alloy. Materials Today, 2017, 4(8): 7365–7374.

[15] Razaq A, Yin Y J, Zhou J X, et al. Influence of alloying elements Sn and Ti on the microstructure and mechanical properties of gray cast iron. Procedia Manufacturing, 2019, 37: 353–359.

[16] Razaq A, Zhou J X, Hussain T, et al. Effect of alloying elements W, Ti, Sn on microstructure and mechanical properties of gray iron 220. China Foundry, 2019, 16(6): 393–398.

[17] Pierce D, Haynes A, Hughes J, et al. High temperature materials for heavy duty diesel engines: Historical and future trends. Progress in Materials Science, 2019,103(6): 109–179.

[18] Tokaji K, Horie T, Enomoto Y. Roles of microstructure and carbides in fatigue crack propagation in high V-Cr-Ni cast irons. Journal of Materials Processing Technology, 2007, 190(1–3): 81–88.

[19] Wang S Q, Wei M X, Wang F, et al. Transition of mild wear to severe wear in oxidative wear of H21 steel. Tribology Letters, 2008, 32(2): 67–72.

[20] Ye F X, Hojamberdiev M, Xu Y H, et al. Volume fraction effect of V_8C_7 particulates on impact toughness and wear performance of V_8C_7/Fe monolithic composites. Journal of Materials Engineering and Performance, 2014, 23(4): 1402–1407.

[21] Yang J, Cai X L, Fu Y H, et al. Evaluation of growth behaviour of vanadium carbides-reinforced iron-based surface compound layer by in-situ reaction. Vacuum, 2019, 166: 178–183.

[22] Wang Y S, Ding Y C, Wang J, et al. In situ production of vanadium carbide particulates reinforced iron matrix surface composite by cast-sintering. Materials & Design, 2007, 28(7): 2202–2206.

[23] Ghasali E, Shirvanimoghaddam K, Alizadeh M, et al. Ultra-low temperature fabrication of vanadium carbide reinforced aluminum nano composite through spark plasma sintering. Journal of Alloys and Compounds, 2018: 433–445.

[24] Aguirre M V, Martín A, Pastor J Y, et al. Mechanical properties of Y_2O_3-doped W-Ti alloys. Journal of Nuclear Materials, 2010, 404(3): 203–209.

[25] Lyu Y, Sun Y, Liu S, et al. Effect of tin on microstructure and mechanical properties of compacted graphite iron. International Journal Cast Metals Research, 2015, 28(5): 263–268.

[26] Wang W, Jing T F, Gao Y W, et al. Properties of a gray cast iron with oriented graphite flakes. Journal of Materials Processing Technology, 2007, 182(1–3): 593–597.

[27] Lyu Y Z. Abrasive wear of compacted graphite cast iron with added tin. Metallography, Microstructure, and Analysis, 2019, 8(1): 67–71.

[28] Kumar P, Bhargava A, Prasad Y V S S, et al. Effect of tin additions on microstructure and mechanical properties of sand casting of AZ92 magnesium base alloy. Journal of Information Security Research, 2013, 10(2): 111–117.

[29] Lv Y, Sun Y, Zhao J, et al. Effect of tungsten on microstructure and properties of high chromium cast iron. Materials & Design, 2012, 39(8): 303–308.

[30] Zhong L S, Zhang S X, Wang X, et al. The investigation on friction and wear properties of cast iron matrix surface compact vanadium carbide layer. Vacuum, 2020, 178: 109467.

[31] Cruz A S, Jacuinde A B, Guerra F V, et al. Microstructural modification of a static and dynamically solidified high chromium white cast iron alloyed with vanadium. Results in Materials, 2020, 7: 100114.

[32] Ahiale G K, Choi W D, Suh Y, et al. Effects of MC-type carbide forming and graphitizing elements on thermal fatigue behavior of indefinite chilled cast iron rolls. Metallurgical and Materials Transactions A, 2015, 46(11): 4819–4827.

[33] Abbasi H R, Bazdar M, Halvaee A. Effect of phosphorus as an alloying element on microstructure and mechanical properties of pearlitic gray cast iron. Materials Science & Engineering A, 2007, 444(1): 314–317.

[34] Liu Y Z, Li Y F, Xing J D, et al. Effect of graphite morphology on the tensile strength and thermal conductivity of cast iron. Materials Characterization, 2018, 144: 155–165.

[35] Yang X, Zhang Z H, Wang J T, et al. Investigation of nanomechanical properties and thermal fatigue resistance of gray cast iron processed by laser alloying. Journal of Alloys and Compounds, 2015, 626: 260–263.